Study on Unsteady Pressure due to Fan Rotor-Stator Interaction

S. Goto, H. Kodama, N. Tsuchiya and Y. Nakamura
Ishikawajima-Harima Heavy Industries Co., Ltd.,
229, Tonogaya, Mizuho-machi, Nishitama-gun, Tokyo 190-1297, JAPAN

O. Nozaki, T. Nishizawa and K. Yamamoto
Japan Aerospace Exploration Agency,
7-44-1 Jindaijihigashi, Chofu, Tokyo, 182-8522, JAPAN

Keywords : CFD, Rotor-Stator Interaction, Noise

Abstract

This paper describes the characteristics of the unsteady pressure on the stator surface induced by rotor viscous wakes. The primary object of this study is to investigate the effects of axial spacing between the rotor and the stator and three-dimensional vane geometries such as stator sweep and stator lean on the unsteady pressure fluctuations on the stator vane.

To predict these fluctuations, unsteady three-dimensional Navier-Stokes analyses are performed. Furthermore, a three-dimensional analytical method using unsteady lifting-surface theory is also used to elucidate the mechanism of interaction of passing rotor wakes with downstream stator.

Five different fan configurations with three sets of stator geometries, which are three radial stator configurations with different axial spacing, the swept stator and the swept and leaned stator, are used for this study.

It is found that, in axial spacing between rotor and stator, the effect of radial phase skew of incoming rotor wake is important for the reduction of the induced unsteady pressure in addition to the rotor wake decay. It is also shown that incorporation of stator sweep and lean is effective to reduce this unsteady pressure.

Nomenclature

L axial distance between rotor and stator
R radius
V absolute velocity at rotor exit
V_t swirl component of V
V_x axial component of V
θ change in the circumferential phase angle of rotor wake during the wake convection from rotor leading edge to stator leading edge
$d\theta$ difference in the circumferential phase angle of rotor wake between hub and tip at stator inlet
Ω angular velocity of rotor rotation

Introduction

ESPR project started in 1999 with METI & NEDO support as a 5-year program to develop environmentally compatible technologies for the next-generation SST program in Japan. This project has 3 major subjects; noise suppression, NO_x reduction and CO_2 reduction. ESPR targets are Chapter3-3dB for noise reduction, 25% reduction for CO_2 emission and below 5gram/kg fuel for NO_x emission.

Among the three subjects, noise suppression is a very important subject. In case of Concorde, the special deviation from ICAO and/or FAA regulations is allowed, which is corresponding to the noise level 15dB above normal subsonic aircraft's. It is thought the noise regulations become more stringent in future not only for subsonic transport but also for supersonic transport. That is the reason why the project target is set minus 3dB below the current noise regulation of ICAO Chapter3 for fan noise at approach and jet noise at sideline, respectively.

A principal source of fan noise is the interaction of fan rotor viscous wakes with stator vanes. In order to achieve the ESPR target for fan noise reduction, it is necessary to fully understand the generation mechanism of rotor-stator interaction noise.

In the ESPR program, we have studied the unsteady pressure on the stator surface induced by rotor viscous wakes by means of three-dimensional unsteady Reynolds-averaged Navier-Stokes equations and the unsteady lifting-surface theory [1][2][3]. The two methods applied to five fan configurations to investigate the effects of axial spacing between the rotor and the stator, stator sweep and stator lean on the unsteady pressures induced by the rotor viscous wakes on the stator vanes.In this paper, the findings obtained so far are presented.

Numerical Analysis

The governing equations are the time-dependent three-dimensional Reynolds-averaged Navier-Stokes equations, and the turbulent viscosity is determined by the two-layer Baldwin-Lomax algebraic turbulence model. An implicit finite difference scheme, which is capable of using large CFL numbers, is used for time integration. The convection terms are discretized using the TVD scheme developed by Chakravarthy and Osher and central differencing is used for the diffusion terms. For the implicit time integration approach, a Newton sub-iteration is performed at each time step to increase stability and reduce linearization errors.A computational domain is divided into sub-domains. The algorithm in the present code is paralleled so that each sub-domain is executed on a different processing element of scalar-paralleled super computer system called Numerical Simulator III in Japan Aerospace Exploration Agency, and exchanges the boundary information with neighboring sub-domains.

Fan Configurations

The major design parameters of a model fan is shown in Table 1. The computational domain is reduced to a 1/9 sector of the annulus with 2 rotor blades and 5 stator vanes. The fan operation conditions for the studies are shown in Table 2. These operation conditions are selected so that similar velocity triangles between 80 and 100 percent rotation speed are obtained at rotor exit.

Figure 1 shows an example of the computational grid for the unsteady stage analysis, in which total number of grids is about 4 million.

Table1. Major design parameters of a model fan

Number of Rotor Blade	18
Number of Stator Vane	45
Hub to Tip Ratio	0.55
Tip Chord Length	0.193

Table2. Fan operating condition

	100%N	80%N
Axial Flow Mach Number	0.5	0.4
Rotor Tip Mach Number	1.15	0.92

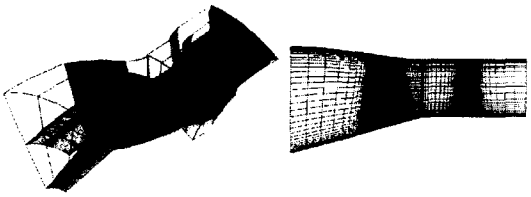

a) 3D view b) Meridional view

Figure1. Computational grid

The stator configurations for the studies are shown in Figure 2. The figure 2a) shows three radial stator configurations, which use the same stator geometry, with different axial distance between the rotor and the stator. The stator located at the shortest axial distance (0.5 rotor axial chord) is the baseline stator (A01). The other two stators are moved downstream. The stator (A02) is located downstream at 1.0 axial chord, and the stator (A03) is at 1.5 axial chord. The figure 2b) shows two three-dimensional geometries; swept (B01) and swept and leaned (C01) stator. The swept stator (B01), in which the stator has 20 degrees of sweep, has the same axial distance as the baseline stator (A01) at the hub and almost the same axial distance as the radial stator (A02) at the tip. And in the swept and leaned stator (C01), a stator lean of 30 deg in the direction of rotor rotation is incorporated into the swept stator (B01) for the upper 70 percent of the span.

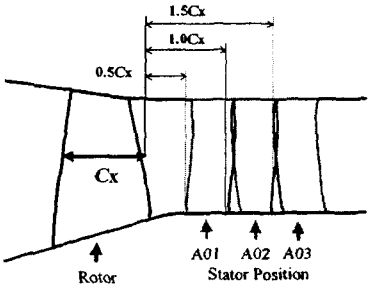

a) Study on axial spacing between rotor and stator

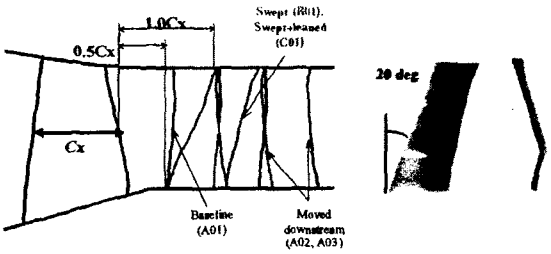

b) Study on swept and swept-leaned stator

Figure2. Stator configurations

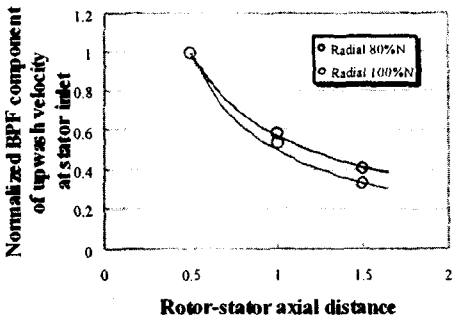

Figure 3. Comparison of radially averaged magnitudes of the upwash velocity at stator inlet.

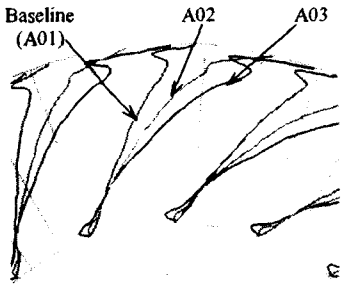

Figure 4. Rotor wakes at stator inlet at 100% rotation speed.

Results and Discussions

The effect of Axial spacing between rotor and stator

Figure 3 shows a comparison of the radially averaged magnitudes of the upwash component of the disturbance velocity between three radial stator configurations at 80 and 100 percent rotation speeds. The average magnitude is normalized by that of the baseline stator (A01) for each rotation speed. This figure shows that the average magunitude of upwash velocity decreases in accordance with a power law.

Rotor wake lines at stator inlet are shown in Figure 4. Radial phase skewing of the rotor wake can be seen in this figure. The radial skew of the wake is increased as the axial spacing is increased.

Figure 5 shows rotor and radial stator on a blade-to-blade plane. A time required for the rotor wake to convect from the rotor trailing edge to the stator leading edge is given by L / V_x. Therefore the change in circumferential phase angle of the wake during the convection can be represented by

$$\theta = V_t \cdot \left(\frac{L}{V_x}\right) \cdot \left(\frac{1}{R}\right) \tag{1}$$

A fan rotor is usually designed that V_x at hub is nearly equal to V_x at tip, then the difference in the circumferential phase angle between the hub and the tip can be expressed in the form

$$d\theta = \theta_{hub} - \theta_{tip} = \left\{\left(\frac{V_t}{R}\right)_{hub} - \left(\frac{V_t}{R}\right)_{tip}\right\} \frac{L}{V_x} \tag{2}$$

From this equation, it is found that the variation in a radial phase skew of the rotor wake with the axial spacing is attributed to the difference in an angular velocity V_t / R between the hub and the tip and that the radial phase skew varies in proportion to the axial distance L.

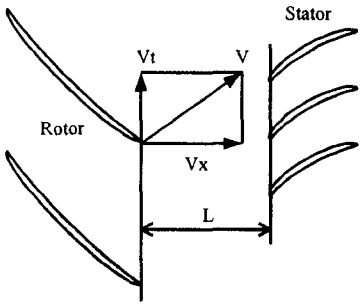

Figure 5. Schematic view of rotor and stator

The differences in the circumferential phase angle of a single rotor wake between the tip and the hub are compared in Figure 6. The numerical calculation results show almost linear variation in the radial phase skew with increasing axial distance for both 80 and 100 percent rotation speed as indicated by equation (2). The results also show the same level of the radial skew between 80 and 100 percent rotation speed for each axial spacing. It is understandable from equation (2), because the numerical calculation results showed a similar swirl angle (that is V_x / V_t) at rotor exit between 80 and 100 percent rotation speed.

In Figure 7, overall amplitudes of the BPF component of unsteady pressure difference across the stator vane, which were obtained by area-averaging of the local BPF amplitude over the stator surface, are compared between three radial stator configurations for both 80 and 100 percent rotation speed. The average amplitude is again normalized by that of the baseline stator (A01) for each rotation speed. In a quantitative comparison, the overall amplitudes obtained from the numerical calculation were considerably larger than those from the analytical calculation, however a comparison of the rate of decrease in the overall amplitude with increasing axial distance from the baseline stator shows a good agreement between the numerical calculation and the analytical calculation. Both predictions show that the rate of decrease in the unsteady pressure with increasing axial distance is larger than the rate of decay in the incoming upwash velocity (red line in the figure) for 80 percent rotation speed, whereas it is smaller for 100 percent rotation speed. In the lifting surface theory used in the analytical calculation, the effect of the magnitude of upwash velocity on the amplitude of unsteady pressure difference is linear. Therefore a remarkable difference in the rate of unsteady pressure reduction between these two rotation speeds is considered to be attributed to the effect of radial phase skew of the rotor wake.

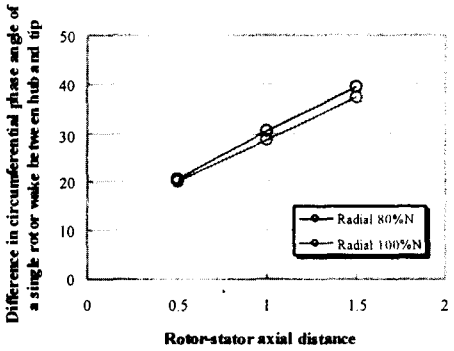

Figure 6. Comparison of a radial phase of skew

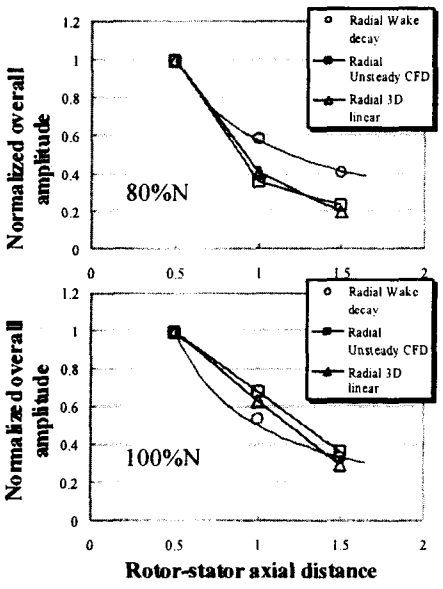

Figure 7. Comparison of overall amplitudes of unsteady pressure difference

In order to clarify the effect of the phase skew of incoming rotor wake on the unsteady pressure difference, further calculations using the analytical method, in which only a phase skew of incoming rotor wake is varied with keeping upwash velocity component constant, were conducted for both 80 and 100 percent rotation speeds. Figure 8 shows the variation of resulting overall amplitude of unsteady pressure difference with the difference in the circumferential phase

angle between the hub and the tip $d\theta$. In the figure, the overall amplitude is normalized by that at the $d\theta$ of baseline stator (A01) in Figure 6 for each rotation speed (around 20 deg for both rotation speeds). It is found that the amplitude of unsteady pressure difference has a peak value at a certain $d\theta$ and the $d\theta$ at the peak differs depending on a rotation speed. The peak of 80 percent rotation speed locates near the $d\theta$ of baseline stator (A01), so the unsteady pressure difference decreases at larger $d\theta$, that is, $d\theta$ of radial stator (A02) and radial stator (A03). On the other hand, the peak of 100 percent rotation speed locates near the $d\theta$ of radial stator (A02), therefore the unsteady pressure difference once increases from the $d\theta$ of baseline stator (A01) to the $d\theta$ of radial stator (A02) and then decreases. The consequent level of the unsteady pressure difference at the $d\theta$ of radial stator (A03) is not much different from that at the $d\theta$ of baseline stator (A01). These variations can clearly explain the reason why the reduction in unsteady pressure difference with increasing axial distance is significantly large compared with the decay in the incoming upwash velocity for 80 percent rotation speed, while the reduction is unexpectedly small for 100 percent rotation speed.

From the above investigations for the radial stator configurations with different rotor-stator spacing, it can be said that the effect of radial phase skew of incoming rotor wake should be carefully considered in determining an axial distance between rotor and stator.

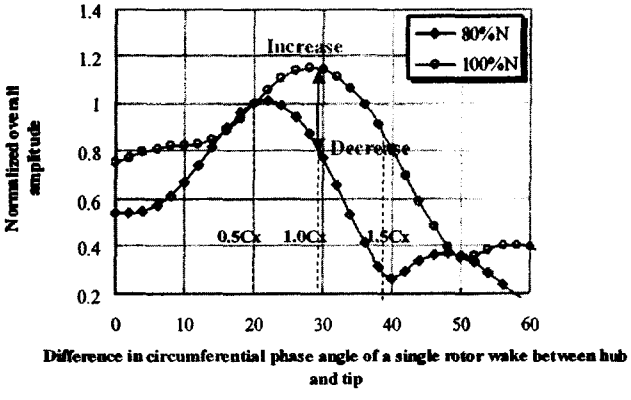

Figure 8. Variation of overall amplitude of unsteady pressure difference with the difference in circumferential phase angle between hub and tip

Stator sweep and lean

The numerical predictions for the swept stator (B01) and the swept and leaned stator (C01) were also conducted for both 80 and 100 percent rotation speed. These two stators have the same sweep so that the stator leading edges are located at the same axial position along the span. The backward displacement of the leading edge from the baseline stator (A01) leading edge position allows the rotor wakes to decay further. Figure 9 shows that the radially averaged magnitudes of the upwash velocity for both the swept stator and the swept and leaned stator are considerably decreased from the baseline stator (A01), but still larger than that for the radial stator (A02).

The radial phase skewing is also increased by a stator sweep as shown in Figure 10, but the reason is different from that in the case of a moved downstream radial stator. A schematic view of swept stator and the notation are shown in Figure 11. In the case of a backward swept stator, a time required for the rotor wake to convect from the rotor trailing edge to the stator leading edge at tip is longer than that at hub.

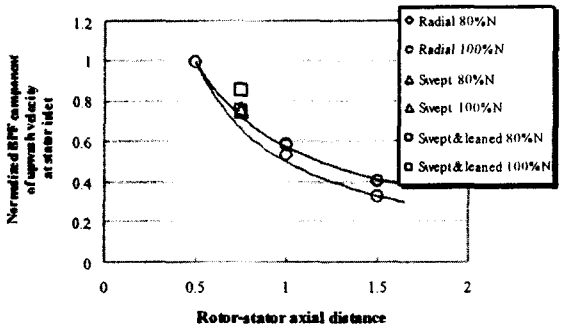

Figure 9. Comparison of radially averaged magnitudes of the upwash velocity at stator

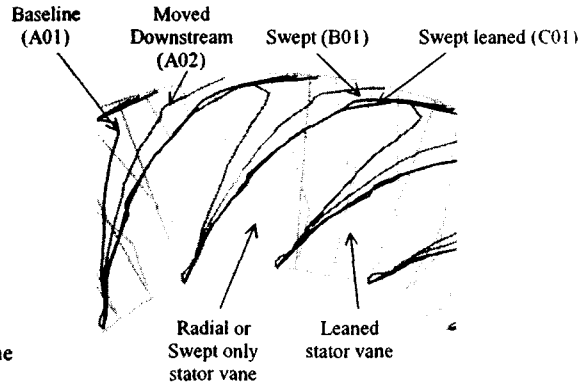

Figure 10. Rotor wakes at stator inlet at 100% rotation speed.

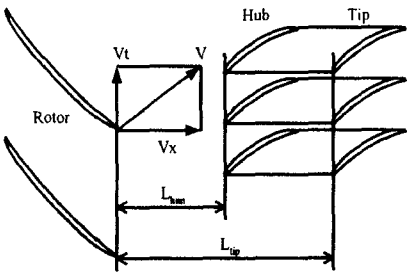

Figure 11. Schematic view of rotor and stator

Therefore the tip portion of the rotor wake that has reached to the stator leading edge was discharged from the rotor trailing edge earlier than the hub portion that has reached to the stator leading edge at the same time. Then the change in the circumferential phase angle of the wake at tip from the circumferential position when the hub portion of the wake was discharged from the rotor trailing edge can be represented by

$$\theta_{tip} = V_{t,tip} \cdot \left(\frac{L_{tip}}{V_x}\right) \cdot \left(\frac{1}{R}\right) - \Omega \cdot \left(\frac{L_{tip} - L_{hub}}{V_x}\right) \qquad (3)$$

Using the same assumption used in equation (2), the difference in the circumferential phase angle between the hub and the tip can be expressed in the form

$$d\theta = \theta_{hub} - \theta_{tip}$$

$$= \left\{\left(\frac{V_t}{R}\right)_{hub} - \left(\frac{V_t}{R}\right)_{tip}\right\}\frac{L_{hub}}{V_x} + \left\{\Omega - \left(\frac{V_t}{R}\right)_{tip}\right\}\frac{L_{tip} - L_{hub}}{V_x} \qquad (4)$$

or

$$\left\{\left(\frac{V_t}{R}\right)_{hub} - \left(\frac{V_t}{R}\right)_{tip}\right\}\frac{L_{tip}}{V_x} + \left\{\Omega - \left(\frac{V_t}{R}\right)_{hub}\right\}\frac{L_{tip} - L_{hub}}{V_x} \qquad (5)$$

The $d\theta$ of the baseline stator (A01) and the second term is positive, because the angular velocity of rotor rotation is larger than the angular velocity of the swirl at tip. This indicates that the $d\theta$ of swept stator is larger than the $d\theta$ of baseline stator (A01). It is also indicated by equation (5) that the $d\theta$ of swept stator is still larger than the $d\theta$ of baseline stator (A02), because the positive second term, where the angular velocity of rotor rotation is still larger than the angular velocity of the swirl at hub in the current fan model, is added to the first term which is equivalent to the $d\theta$ of the radial stator (A02). As seen in Figure 12, the resultant phase differences between the tip and the hub of swept stators obtained from the numerical calculations are larger than that for the baseline stator (A01), and still larger than that for the radial stator (A02) as indicated by equation (4) and (5).

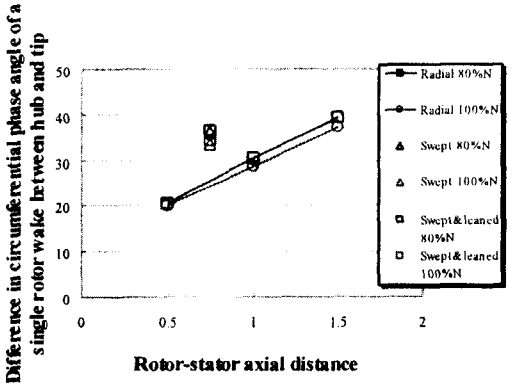

Figure 12. Comparison of the radial phase of skew

Stator lean makes a difference in the number of individual rotor wakes that intersect a given stator vane. Figure 13 shows that the number of intersections is increased by one in the case of the swept and leaned stator compared with the swept stator.

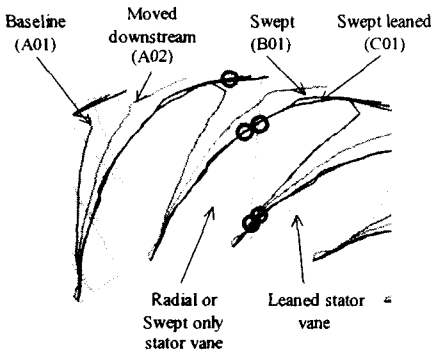

Figure 13. Wake intersections at stator inlet

In Figure 14, overall amplitudes of the BPF component of unsteady pressure difference across the stator vane for the swept stator and the swept and leaned stator are compared with the radial stator configurations (A01 and A02) for both 80 and 100 percent rotation speed. The average amplitude is again normalized by that of the baseline stator (A01) for each rotation speed. A significant decrease in the unsteady pressure difference from the baseline stator (A01) is shown for the swept stator (B01), but the rate of the decrease is different between 80 and 100 percent rotation speed. This may be due to the

difference in variation of unsteady pressure difference with increasing $d\theta$ between two rotation speeds, as observed in the radial stator configurations. As seen in Figure 9, the radially averaged magnitudes of upwash velocity for the swept stator (B01) are larger than those of the radial stator (A02) (about 30 and 40 percent larger, respectively, for 80 and 100 percent rotation speed) whereas the area-averaged amplitudes of unsteady pressure difference for the swept stator (B01) are about 20 percent smaller than those of the radial stator (A02) for both 80 and 100 percent rotation speed. The difference in the $d\theta$ between the swept stator (B01) and the radial stator (A02) seems to be too small (only about 5 deg for both 80 and 100 percent rotation speeds as seen in Figure 12) to explain that the difference in the amplitude of unsteady pressure between them is all attributed to the effect of increased radial phase skew of rotor wake. In a swept stator, there may be other beneficial effect for the unsteady pressure reduction than the effects of decay in rotor wake and increase in radial phase skew of rotor wake due to blade sweep.

It can be found from Figure 14 that the unsteady pressure reduction due to incorporation of lean in the swept stator is about 20 percent for both 80 and 100 percent rotation speed.

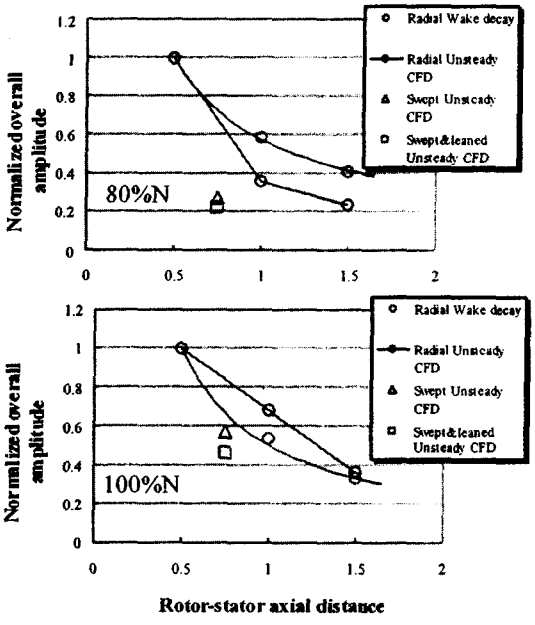

Figure 14. Comparison of radially averaged magnitudes of the upwash velocity at stator

Conclusions

1. Three-dimensional unsteady numerical analysis and theoretical analysis were performed to investigate the unsteady pressure due to rotor-stator interaction.
2. In axial spacing between rotor and stator, the effect of radial phase skew of incoming rotor wake takes an important role in the reduction in the induced unsteady pressure. However increasing the radial phase skew doesn't always decrease the unsteady pressure.
3. It is indicated that, in the use of a swept stator, there may be other beneficial effect for the unsteady pressure reduction than the effects of decay in rotor wake and increase in radial phase skew of rotor wake due to the blade sweep.

Acknowledgement

The authors would like to express their thanks to the New Energy and Industrial Technology Development Organization (NEDO) and the Ministry of Economy, Trade and Industry (METI), who gave them the opportunity to conduct "Research and Development of Environmentally Compatible Propulsion System for Next-Generation Supersonic Transport (ESPR) project".

References

[1] Tsuchiya, N., Nakamura, Y., Yamagata, A., and Kodama, H., Nozaki, O., Nishizawa, T., and Yamamoto, K., "Fan Noise Prediction Using Unsteady CFD Analysis," AIAA-2002-2491, 2002.

[2] Tsuchiya, N., Nakamura, Y., Yamagata, A., and Kodama, H., Nozaki, O., Nishizawa, T., and Yamamoto, K., "Investigation of Acoustic Modes Generated by Rotor-Stator Interaction," AIAA-2003-3136, 2003.

[3] Yamagata, A, Tsuchiya, N., Nakamura, Y., Yamagata, A., and Kodama, H., Nozaki, O., Nishizawa, T., and Yamamoto, K., "CFD Prediction of Unsteady pressures due to Fan Rotor-Stator Interaction," ISABE-2003-1130.